Applied Catalysis B: Environmental 142–143 (2013) 268–277

Contents lists available at SciVerse ScienceDirect

Applied Catalysis B: Environmental

journal homepage: www.elsevier.com/locate/apcatb

Study on the selective catalytic reduction of NO with toluene over $CuO/CeZrO_2$. A confirmation for the three-function model of HC-SCR using the temperature programmed methods and in situ DRIFTS

Agata Łamacz*, Andrzej Krztoń, Gérald Djéga-Mariadassou

Polish Academy of Sciences, Centre of Polymer and Carbon Materials, Marii Curie-Skłodowskiej 34, 41-819 Zabrze, Poland

ARTICLE INFO

Article history:
Received 27 July 2012
Received in revised form 10 May 2013
Accepted 16 May 2013
Available online 23 May 2013

Keywords:
HC-SCR
Three-function model
DRIFTS
Ceria-zirconia
Toluene

ABSTRACT

This paper deals with the selective catalytic reduction of NO with the use of toluene as a reducer and in the presence of excess oxygen. The three-function model of HC-SCR of NO has been studied over ceria-zirconia supported copper oxide ($CuO/CeZrO_2$). The particular functions of $CuO/CeZrO_2$ catalyst have been proved by the catalytic runs carried out in temperature-programmed conditions (TPSR) and in situ DRIFTS. On the basis of obtained results it was observed that NO is oxidized by O_2 to NO_2, which is subsequently used for toluene activation. Obtained oxygenates ($C_xH_yO_z$) clean the active sites from oxygen, which was left during NO reduction to N_2. The DRIFTS studies have shown that NO adsorbs on the surface of ceria-zirconia forming (i) the bridging nitrate when the adsorption of NO is carried out in the absence of gaseous O_2 and (ii) both nitrite and nitrate species when the adsorption is carried out in the presence of O_2. Formation of these surface species can be due to the presence of surface peroxide species (O_2^{2-}) or superoxide species (O^{2-}). The presence of the latter enhances NO adsorption and influences the evolution of surfaces species during temperature programmed reaction.

1. Introduction

Nitrogen oxides (NO_x) are formed in combustion processes in power stations and in vehicles. Except NO_x, volatile organic compounds (VOCs) and polycyclic aromatic hydrocarbons (PAHs) are released to the atmosphere [1]. The amount of these pollutants in the flue gases from coal combustion depends on the type of coal and the excess of oxygen used in combustion process. The application of approximately 4% of oxygen above 800 °C leads to 110 ppm of NO_x and mg/Nm^3 of both VOCs (mainly aromatic hydrocarbons, e.g. BTX) and PAHs [2]. Therefore, NO_x removal from the exhaust gases may be carried out by the selective catalytic reduction (SCR) with the use of hydrocarbon, which is an "internal" reductant. Beside HC-SCR, there are also other, widely studied and applied catalytic methods of NO_x abatement, e.g. H_2-SCR [3] or NH_3-SCR [4,5]. During direct decomposition of NO_x to N_2 and O_2 (without additional reagents as HC or NH_3), the NO_2 and N_2O are always the byproducts and the selectivity to N_2 and O_2 is relatively low [6,7]. Moreover, NO_x decomposition requires high temperatures (above 600 °C) and the catalysts characterize with poor stability in the presence of H_2O or SO_2. This paper deals with NO_x decomposition assisted by hydrocarbons. The issue of catalytic NO_x removal has been widely studied on zeolite based catalysts [8–11] or Al_2O_3, TiO_2, SiO_2, CeO_2 supported Co, Ni, Au, Ag, Pt, Rh, Pd [12–15]. These catalysts revealed good activity in HC-SCR, however they deactivate in the presence of H_2O and SO_x [16]. In the last decade, ceria-zirconia mixed oxides have attracted much attention due to their unique redox properties and high OSC, and the possibility of their potential application in the industrial scale NO_x abatement. Recent studies have shown that ceria-zirconia supported metal catalysts are very active in selective catalytic reduction of NO_x by hydrocarbons [17–19]. One of the mechanisms of HC-SCR of NO_x assumes surface reaction between adsorbed intermediates (ad-N_xO_y and ad-HC), whose probability to occur at a given temperature depends on the intrinsic reactivity of the catalytic system and local structures of these intermediates [21]. Another mechanism of SCR of NO reaction in the presence of ethanol assumes its oxidation to acetaldehyde. Surface acetaldehyde ion reacts with NO_2 to yield nitromethane that dissociates to isocyanates ions (NCO^-) that is a precursor for NH_3. Therefore, further HC-SCR mechanism is similar to NH_3-SCR [15].

Djéga-Mariadassou [21] proposed the model of HC-SCR reaction in which NO_x decomposition in the presence of hydrocarbon proceeds according to three assisted catalytic cycles. The model considers three following functions:

F1: oxidation of NO to NO_2 (Eq. (2)), taking place on metal oxide;
F2: mild oxidation of HC by NO_2 to oxygenate compounds ($C_xH_yO_z$) via nitro compounds (RNO_x) [22] (Eq. (3));

* Corresponding author. Tel.: +48 032 2716077; fax: +48 032 2382831.
E-mail address: agata.lamacz@cmpw-pan.edu.pl (A. Łamacz).

0926-3373/$ – see front matter © 2013 Elsevier B.V. All rights reserved.
http://dx.doi.org/10.1016/j.apcatb.2013.05.030

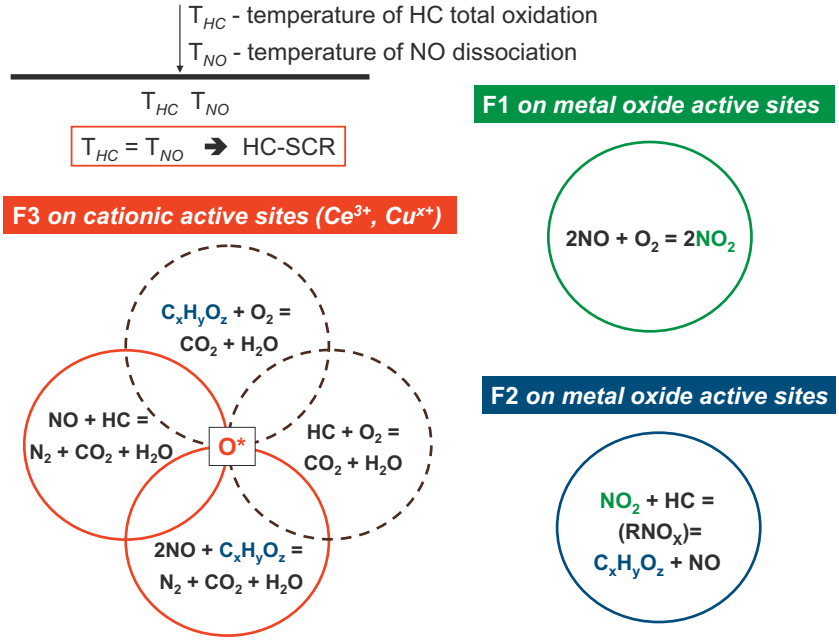

Fig. 1. Three functions of HC-SCR turn over at the same temperature ($T_{HC} = T_{NO}$). The effect of competitive total oxidations of hydrocarbon and oxygenates (—), which are kinetically coupled with two cycles of F3 (——), i.e. reduction of NO assisted by HC or $C_xH_yO_z$. (For interpretation of the references to color in this figure legend, the reader is referred to the web version of the article.)

F3: dissociation of two molecules of NO on cationic active sites (*) via adsorbed dinitrosyl species [23] what yields N_2 and leaves two adsorbed oxygen species (Eq. (4)). This oxygen is utilized in reaction of oxygenates ($C_xH_yO_z$) total oxidation to CO_2 and H_2O, providing regeneration of the active site (*) (Eq. (5)). An overall reaction of this function is described by Eq. (6).

$$2NO + \text{reductant} + O_2 = N_2 + CO_2 + H_2O \quad (1)$$

$$NO + \tfrac{1}{2}O_2 = NO_2 \quad (2)$$

$$NO_2 + HC \rightarrow (RNO_x) \rightarrow NO + C_xH_yO_z \quad (3)$$

$$2NO + 2* = N_2 + 2O* \quad (4)$$

$$\text{“oxygenates”} + 2O* \rightarrow CO_2 + H_2O + 2* \quad (5)$$

$$2NO + \text{“oxygenates”} \rightarrow N_2 + CO_2 + H_2O \quad (6)$$

Described above three functions have to turn over simultaneously at the same temperature because the first function delivers NO_2 to F2 and the second function provides oxygenate compounds to F3. The $C_xH_yO_z$ cleans the surface from oxygen species left by NO dissociation, so the active sites are regenerated and the reduction–decomposition of NO to N_2 can still occur. In such a case the F3 is described by the following global Eq. (7):

$$C_xH_yO_z + (2x + \tfrac{1}{2}y - z)NO = (x + \tfrac{1}{4}y - \tfrac{1}{2}z)N_2 + xCO_2 + \tfrac{1}{2}yH_2O \quad (7)$$

When the HC is active at the temperature of NO dissociation, the oxygen species are scavenged by HC and the HC-SCR reaction takes place according to the third function (F3) (Eq. (8)).

$$C_xH_y + (2x + \tfrac{1}{2}y)NO = (x + \tfrac{1}{4}y)N2 + xCO_2 + \tfrac{1}{2}yH_2O \quad (8)$$

The co-existence of F1, F2 and F3 (Fig. 1) depends on the nature of reducer and chemical composition of the catalyst. Reaction of total oxidation of $C_xH_yO_z$ by O* (to CO_2 and H_2O) proceeds easier than reaction of total oxidation of HC. Therefore, F1 and F2 play important role in HC-SCR of NO. Depending on the chemical composition of the catalyst, the competitive reactions – i.e. the oxidation of HC or $C_xH_yO_z$ to CO_2/H_2O (marked broken lines in Fig. 1) – can occur on cationic active sites. In such a case, the consumption of reductant leads to strong decrease of NO_x conversion. Hydrocarbon and oxygenates can go though their total oxidations to CO_2/H_2O simultaneously with F1, F2 and F3.

The aim of this paper is to confirm the three-function model of HC-SCR of NO by (i) catalytic runs in temperature programmed conditions and (ii) in situ DRIFTS during temperature programmed desorption of NO (NO-TPD) and HC-SCR reaction over ceria-zirconia supported copper catalyst. Copper based catalysts have attracted much attention for NO_x reduction. The most popular Cu-ZSM-5, which was believed to be most promising catalyst for NO_x decomposition, has one major disadvantage: it is not resistant to H_2O and SO_2 present in flue gases from coal combustion. In the last decade, ceria-zirconia mixed oxides have attracted much attention due to unique redox properties (e.g. high oxygen storage capacity (OSC)) and possibility of their potential application in NO_x abatement in industrial scale. Recent studies have shown that ceria-zirconia supported metal or metal oxides catalysts are very active in selective catalytic reduction of NO_x by hydrocarbons [18,24]. For the copper supported on ceria-zirconia the formation of strong specific copper–support interactions was observed [25]. Furthermore, copper-based catalysts are environmentally compatible and economically advantageous.

In our work we use toluene as a model reductant for studied reaction because this hydrocarbon is present in the flue gases from coal combustion. The assumptions of the three-function model of HC-SCR of NO have been proved by the catalytic runs in temperature-programmed conditions (which give information about temperatures for F1, F2 and F3) and by the DRIFTS, which permits to identify surface species formed on $CuO/CeZrO_2$ in the atmosphere of $NO + O_2$, C_7H_8 or $NO + O_2 + C_7H_8$.

2. Experimental

2.1. Catalyst synthesis and characterization

The catalyst containing 4 wt.% of copper was prepared by the impregnation of commercial ceria-zirconia support ($Ce_{0.63}Zr_{0.37}O_2$; Rhodia Electronics) with aqueous solutions of copper nitrate ($Cu(NO_3)_2{\cdot}6H_2O$). Obtained $CuO/CeZrO_2$ catalyst was dried at 120 °C and calcined in air at 550 °C for 2 h.

The high-resolution transmission electron microscopy (HRTEM) was performed on the JEOL-JEM 2011 HR apparatus, associated with a top entry device and operating at 200 kV.

2.2. Catalytic runs

Temperature programmed desorption of NO (NO-TPD) and temperature programmed surface reactions (TPSR) were performed in a U-type reactor placed in an oven with temperature regulator. The outlet gas was analyzed using the specific detectors. The NO_x (NO and NO_2) was detected by a chemiluminescent analyzer (NOXMAT CLD 700 AL). The N_2O, CO_2 and CO were detected by a non dispersive infrared detector (NDIR) (ULTRAMAT 6 E). The concentration of hydrocarbon was detected using the FIDAMAT 5E-I flame ionization detector (FID). Before all catalytic runs, the $CuO/CeZrO_2$ sample was calcined in situ in 5 vol.% O_2/Ar at 550 °C for 2 h.

The NO-TPD experiment was preceded by the adsorption of 250 ppm NO/5 vol.% O_2/Ar at room temperature for 1.5 h and then the sample was purged in Ar for 1 h. NO-TPD was carried out in flowing 5 vol.% O_2 in Ar.

TPSR of NO oxidation (NO_{ox}-TPSR) was carried out in 250 ppm NO/5 vol.% O_2/Ar. TPSR of HC-SCR reaction in the absence of oxygen (NO/HC-TPSR) and in the presence of excess O_2 (NO/O_2/HC-TPSR) were carried out in gas mixtures containing respectively 250 ppm NO/250 ppm C_7H_8/Ar and 250 ppm NO/250 ppm C_7H_8/5 vol.% O_2/Ar.

All catalytic runs were conducted under atmospheric pressure, with the total flow rate of 250 ml/min and heating rate of 3 °C/min from RT up to 500 °C. Gas hourly space velocity (GHSV) was 10,000 h^{-1}.

2.3. DRIFTS

The diffuse reflectance FT-IR measurements (DRIFTS) were carried out in situ in a temperature cell fitted with ZnSe windows and coupled to a BIO-RAD FTS 165 infrared spectrometer with KBr optics. Typically, 256 scans were taken to improve signal to noise ratio. The amount of utilized sample was 30 mg of powder. In order to eliminate surface nitrates and carbonates, catalyst sample was heated in situ at 400 °C for 2 h. The evolution of functional groups on $CeZrO_2$ and $CuO/CeZrO_2$ was observed during NO adsorption (250 ppm NO/5 vol.% O_2/Ar), NO-TPD (carried out in Ar add preceded by 40 min adsorption of 250 ppm NO/5 vol.% O_2/Ar at RT), adsorption of toluene (250 ppm C_7H_8/Ar) and HC-SCR reaction (250 ppm NO/250 ppm C_7H_8/5 vol.% O_2/Ar).

The spectra of catalyst surface in flowing Ar and in reaction mixtures were collected from RT to 450 °C, increasing temperature by 50 °C. The spectra of $CeZrO_2$ and $CuO/CeZrO_2$ in each reaction mixture were referenced to the sample spectra at the same temperature in flowing Ar, discarding in these way thermal effects.

3. Results and discussion

3.1. Catalyst characterization

The XRD and H_2-TPR characterization of $CeZrO_2$ and $CuO/CeZrO_2$ catalyst were presented in our previous paper [26]. The HRTEM observations of $CeZrO_2$ and $CuO/CeZrO_2$ are presented in Fig. 2. It is observed in Fig. 2a, that the average particle size of irregularly shaped ceria-zirconia is 6–10 nm. The spacing of lattice fringes measured perpendicularly to the electron beam corresponds to (2 2 2), (3 1 1) and (4 0 0) planes. The HRTEM image shows some overlapping regions of ceria-zirconia particles, which are very important from the viewpoint of the catalytic properties of $CeZrO_2$. The HRTEM image of $CuO/CeZrO_2$ (Fig. 2b) shows $CeZrO_2$ crystallites oriented in (2 2 2) and (3 1 1) directions, and (1 1 0) and (1 1 2) crystal planes of CuO. The HRTEM also revealed the superposition of one CuO (1 1 0) and two $CeZrO_2$ (3 1 1) crystals. Impregnation of ceria-zirconia with copper nitrate and further calcination may also lead to formation of thin amorphous layer of CuO, which is dispersed on intergranular boundaries [27]. The XRD and H_2-TPR characterization of $CuO/CeZrO_2$ [26] and presented in this work HRTEM observations revealed that copper occurs in the form of dispersed CuO and isolated Cu^{2+} ions, strongly interacting with $CeZrO_2$.

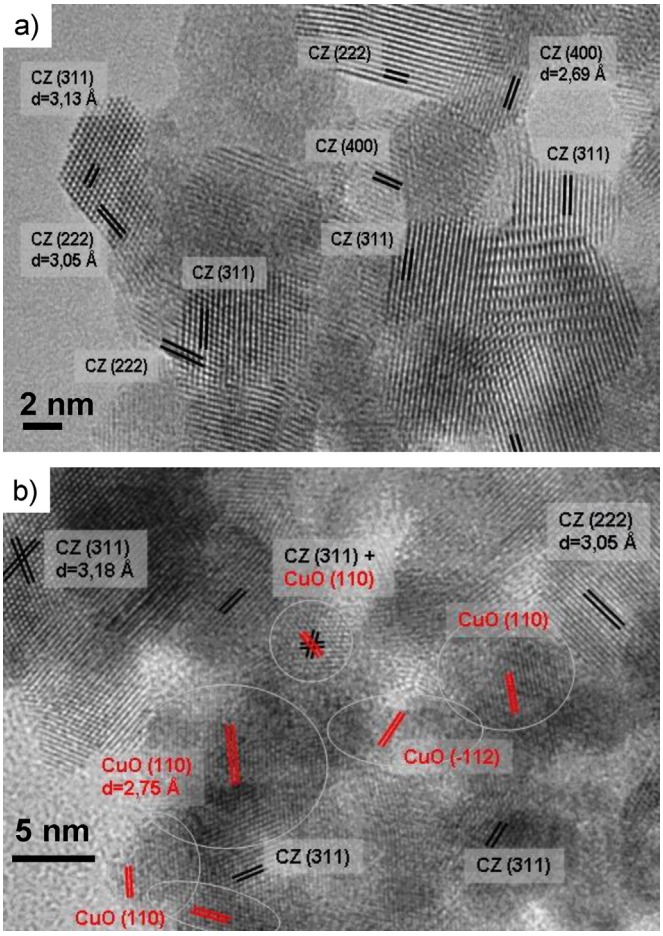

Fig. 2. HRTEM images of (a) $CeZrO_2$ and (b) $CuO/CeZrO_2$.

3.2. Catalytic runs. Confirmation of the "three-function model"

In order to confirm described above mechanism of HC-SCR of NO, four different experiments in the temperature-programmed mode were carried out over $CuO/CeZrO_2$. The evolution of NO and NO_2 during NO-TPD, NO_{ox}-TPSR, NO/HC-TPSR and NO/O_2/HC-TPSR over $CuO/CeZrO_2$ is shown in Fig. 3. Graphs were divided into areas (A, B, C and D) in order to better illustrate the individual tasks of $CuO/CeZrO_2$ during HC-SCR process.

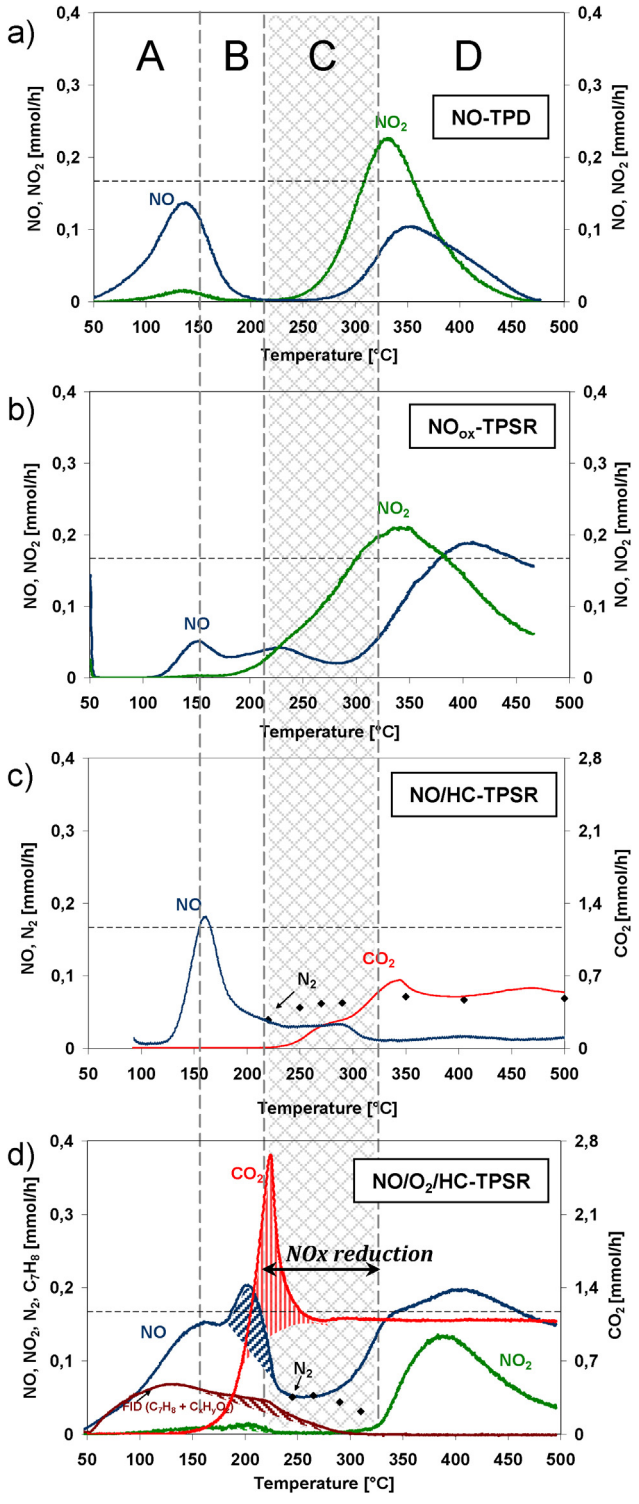

Fig. 3. Catalytic runs of NO-TPD under flowing O_2/Ar, TPSR of NO oxidation (NO_{ox}-TPSR: NO + O_2/Ar), TPSR of NO_x reduction assisted by toluene in the absence of oxygen (NO/HC-TPSR: NO + C_7H_8/Ar) and in the presence of excess oxygen (NO/O_2/HC-TPSR: NO + O_2 + C_7H_8/Ar) over CuO/$CeZrO_2$.

Area "A". It is observed on NO-TPD plot that NO desorbs from the catalysts surface from 50 °C with maximum at ca. 140 °C, what is in agreement with TPSR profiles. Significant adsorption of NO during NO_{ox}-TPSR stems from the fact that reaction mixture consists only of NO and O_2/Ar, whereas smaller adsorption of NO observed on NO/O_2/HC-TPSR profile arises from the presence of the additional compound in reaction mixture, which is toluene. In this case two reagents are competing to CuO/$CeZrO_2$ surface.

Small peak of NO_2 observed at 150 °C on NO-TPD profile is due to NO_2 presence in the NO/Ar cylinder. Desorption of NO during NO_{ox}-TPSR is much smaller than in the case of NO-TPD. Therefore, the amount of NO_2 is hardly detectable. Small amount of NO_2 observed at 150 °C on NO/O_2/HC-TPSR arises from its consumption in reaction of toluene oxidation to RNO_x. At low temperatures RNO_x accumulate on catalyst surface.

Area "B". As is presented in Fig. 3, oxidation of NO to NO_2 (F1) starts above 150 °C. Toluene consumption and CO_2 formation during NO/O_2/HC-TPSR are observed at nearly the same temperature. NO_{ox}-TPSR is an auxiliary experiment, which allows determining the temperature of NO oxidation by gaseous O_2. Formation of NO_2 cannot be observed during NO/O_2/HC-TPSR because just after formation it reacts with hydrocarbon to yield nitro compounds (RNO_x). Decomposition of unstable RNO_x leads to formation of oxygenates ($C_xH_yO_z$) and NO and it shows by the increase in FID signal and NO formation (hatched areas) at ca. 200 °C. Therefore, it proves the occurrence of F2. The second peak of NO desorption is not observed during NO/HC-TPSR. This evidences the role of oxygen in presented model. In the absence of O_2 (NO/HC-TPSR), NO is not oxidized to NO_2; hence, F1 and F2 are not occurring.

Area "C". The concentrations of NO and NO_2 decrease above 215 °C while CO_2 still shows increasing trend. It evidences the occurrence of F3 and indicates the beginning of NO_x reduction. The appreciable increase of CO_2 formation arises from (i) reaction of toluene total oxidation by NO_2 to CO_2/H_2O or (ii) decomposition of RNO_x and subsequent oxidation of $C_xH_yO_z$. Both toluene and RNO_x were accumulated on CuO/$CeZrO_2$ surface at lower temperatures (in area "A"). Significant production of CO_2 in area "C" has not been observed during catalytic runs in steady state experiments (not discussed in this paper) because these experiments were carried out at relatively high temperatures (above 220 °C), preventing the accumulation of toluene and RNO_x, and further overproduction of CO_2.

The temperature of NO_x reduction is attributed to the temperature of NO activation, which is also the temperature of NO desorption from the catalyst surface. It is observed on NO-TPD profile that desorption of NO_2 (produced by oxidation of pre-adsorbed NO) starts at ca. 240 °C. Moreover, the rate of NO oxidation (Eq. (2)) during NO_{ox}-TPSR is the highest from 240 to 290 °C. In the same temperature range on NO/O_2/HC-TPSR profile, one observes that toluene concentration decreases faster than at lower temperatures whereas NO_2 is completely consumed. It indicates the occurrence of F2 (Eq. (9)).

$$C_xH_y + zNO_2 = C_xH_yO_z + zNO \quad (9)$$

Besides, simultaneous formation of CO_2 proves the occurrence of F3 (Eq. (7)). The combination of NO, NO_2 and C_7H_8 consumptions with CO_2 formation evidences that all three functions occur at the same temperature range on CuO/$CeZrO_2$.

The formation of N_2 during NO/O_2/HC-TPSR was determined at 245, 265, 290 and 310 °C, by the μGC analysis of the gas on the reactor outflow. As is presented in Table 1, the selectivity to N_2 was ranging from 88 to 93%.

Table 1
Conversion of NO_x and selectivity to N_2 during NO/O_2/HC-TPSR over CuO/$CeZrO_2$.

Temperature [°C]	NO_x conversion [%]	Selectivity to N_2 [%]
245	67	90
265	67	94
290	59	88
310	42	89

During reaction carried out in the absence of O_2 (NO/HC-TPSR) the formation of CO_2 starts at 225 °C and arises from (i) reduction of NO in the presence of toluene (F3) (Eq. (10)) and (ii) toluene oxidation to CO_2/H_2O by the oxygen from the catalyst, i.e. from CuO and ceria-zirconia.

$$18NO + C_7H_8 = 9N_2 + 7CO_2 + 4H_2O \quad (10)$$

As has been shown on NO_{ox}-TPSR and NO/O_2/HC-TPSR in Fig. 3, in the presence of the excess oxygen, NO and toluene are oxidized to NO_2 and CO_2/H_2O even from 150 °C. In the absence of gaseous O_2 (NO/HC-TPSR), toluene is converted to CO_2/H_2O from 230 °C, and this is exactly the same temperature at which HC-SCR reaction starts to occur in the presence of excess oxygen (NO/O_2/HC-TPSR). Therefore, the presence of oxygen in the gas phase does not decrease the temperature of HC-SCR, but it protects the catalyst from carbon deposition and, when the selection of reducer is proper, enhances NO reduction to N_2. The GC analysis of reaction products during the NO/HC-TPSR run proved formation of N_2 with the selectivity of about 90%. Additionally, the $CuO/CeZrO_2$ has been subjected to a test in the mixture of $NO + C_7H_8$/Ar for 1 h out at 250 °C. During this experiment the selectivity to N_2 was 92%.

Area "D". The increase in NO_2 formation during NO/O_2/HC-TPSR from 290 °C indicates the decrease of NO reduction. Moreover, from 290 °C toluene is being almost completely oxidized to CO_2 and reaction of its total oxidation (Eq. (11)) preponderates over F2 (Eq. (9)).

$$C_7H_8 + 9O_2 = 7CO_2 + 4H_2O \quad (11)$$

The GC–MS analysis at the reactor outlet revealed the traces of naphthalene (at 125 °C) and 1,2,3,4-tetrahydro-5-nitronapthalene (at 125, 215 and 320 °C). The oxidation of NO to NO_2 is observed up to 330 °C during both NO-TPD and NO_{ox}-TPSR experiments. From 330 °C NO_2 starts to decrease because the equilibrium is shifted back to NO and $½O_2$. As presented on NO_{ox}-TPSR profile, no further oxidation of NO occurs.

On the NO/HC-TPSR graph, the conversion of toluene to CO_2/H_2O increases, which results in increase of the number of active sites for NO dissociation (Cu^+ ions and oxygen vacancies in $CeZrO_2$). Therefore, NO reduction to N_2 is higher than that observed in area C.

The results of NO-TPD, NO_{ox}-TPSR, NO/HC-TPSR and NO/O_2/HC-TPSR catalytic runs have shown that HC-SCR of NO with the use of toluene over $CuO/CeZrO_2$ occurs from 215 to 325 °C and that in this temperature range the three functions turnover simultaneously. During all experiments, neither N_2O nor CO has been produced.

3.3. Study of surface species by DRIFTS

In order to complete the fundamental aspects of HC-SCR reaction and confirm the particular functions of the catalyst (F1, F2, F3), the surface of $CuO/CeZrO_2$ was subjected to DRIFTS during NO adsorption, temperature programmed desorption of NO (NO-TPD) and NO reduction with the use of HC.

NO adsorption and NO-TPD. The molecule of NO reacts with the surface oxygen of metal oxides to yield nitrite (NO_2^-) and nitrate (NO_3^-) compounds. The formation of nitrite ion is connected to the transfer of activated oxygen from the surface of ceria to the NO molecule (Eq. (12)). Further transfer of activated oxygen leads to formation of nitrate anion at higher temperatures (Eq. (13)) [28]. Both, the nitrite and nitrate ions are detected by IR.

$$NO + O_2^- \rightarrow NO_2^- + e^- \quad (12)$$

$$NO_2^- + O_2^- \rightarrow NO_3^- + 2e^- \quad (13)$$

Due to the high stability of oxygen vacancy defects, the surface of $CeZrO_2$ contains reduced Ce sites (Ce^{3+}), which are accompanied by oxygen vacancies and can be reoxidized by oxygen from NO molecule or air [29]. If O_2 adsorbs at the top site of Ce^{3+} ion, which is close to the surface oxygen vacancy, it slips into the vacancy and a diamagnetic peroxide species (O_2^{2-}) is formed. When O_2

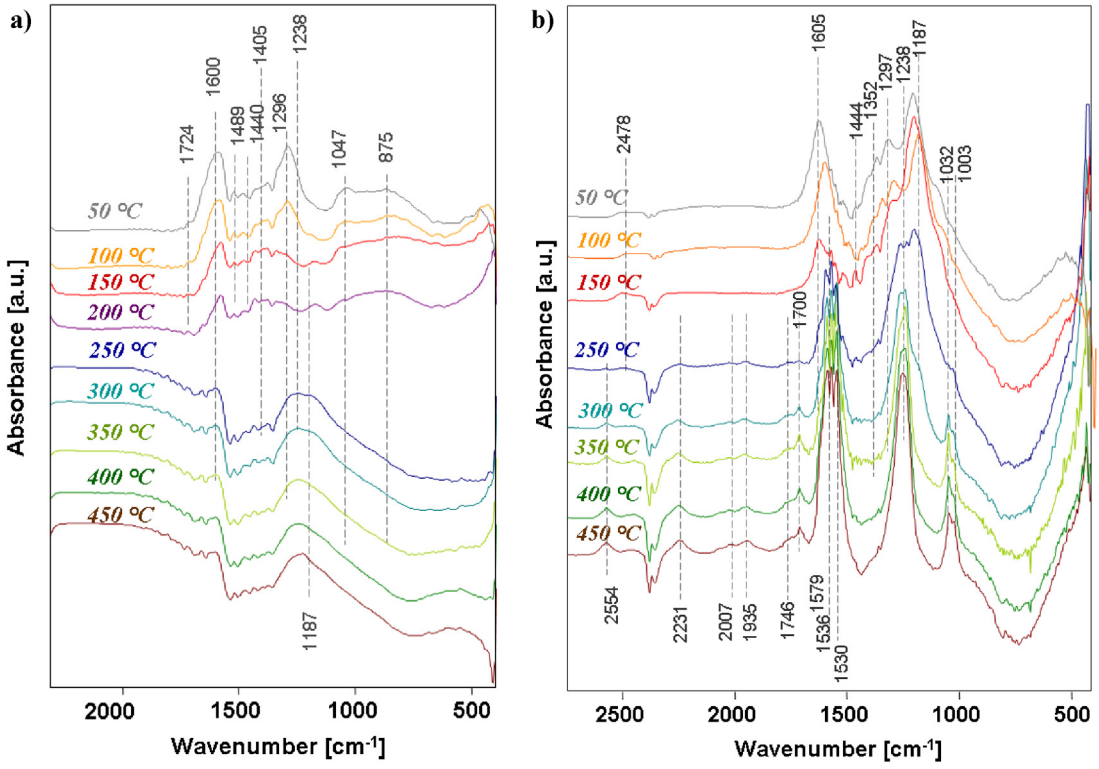

Fig. 4. DRIFTS of $CeZrO_2$ during temperature programmed desorption of NO in Ar after adsorption of (a) 250 ppm NO/Ar and (b) 250 ppm NO + 5 vol.% O_2/Ar.

adsorbs at the top site of Ce^{3+} ion being separated from the surface oxygen vacancy, the superoxide species (O_2^-) are obtained. The super oxides can be easily transformed into peroxides when the temperature is increased [30,31].

The spectral regions for NO adsorption on oxide surfaces occur from 1000 to 1100 cm^{-1} (ν_1) and from 1170 to 1650 cm^{-1} (ν_3). The bands coming from ν_s and ν_{as} vibrations of nitrite occur at 1205–1520 cm^{-1} and 1180–1350 cm^{-1}, respectively [28]. However, the interpretation is complicated because all types of NO_x complexes may give absorption bands in the same frequencies range, i.e. from 1000 to 1600 cm^{-1}.

The DRIFT spectra of pristine $CeZrO_2$ surface during temperature programmed desorption of NO in Ar are presented in Fig. 4. The NO-TPD was preceded by the adsorption of 250 ppm NO/Ar (Fig. 4a) and 250 ppm NO + 5 vol.% O_2/Ar (Fig. 4b) at RT. In Fig. 4a two characteristic bands with medium intensity are observed at about 1600 and 1296 cm^{-1} at low temperatures. These bands can be due to formation of bridging nitrates on ceria-zirconia surface after NO adsorption. The bands at 1047 and 875 cm^{-1} can be attributed to superoxide (O_2^-) and peroxide species (O_2^{2-}) respectively. The superoxides are less stable than peroxides; therefore, simple conversion to peroxide by disproportionation or successively accepting electron from surface can be expected [30,31]. Bands at about 1600 and 1296 cm^{-1} disappear above 200 °C and only one broad band at 1238 cm^{-1} with wide shoulder stretched up to 800 cm^{-1} is observed. The position of this band suggests transformation of bridging nitrate to monodentate nitrate or bridging nitrite since the absorption bands of ν(N=O) are not observed. The appearance of negative band at 3690 cm^{-1} in all temperatures (not shown) is due to reaction of the surface –OH groups, which are present on ceria-zirconia, with adsorbed NO_x species. Such negative bands were observed by many authors [20,29,33]. Fig. 4b shows DRIFT spectra of $CeZrO_2$ during temperature programmed desorption of NO in Ar after pre-adsorption of NO + O_2/Ar at RT. The intensity of vibration bands are stronger than during NO-TPD carried out after adsorption of NO/Ar (Fig. 3a). It was proved by the experiment of NO adsorption in the presence and in the absence of O_2 (Fig. 5), that O_2 enhances adsorption of NO. On the DRIFTS of NO-TPD at 50 °C (Fig. 4b), the absorption bands at 1605, 1297 (ascribed to bridged nitrate) and 1187 cm^{-1} (coming from bidentate nitrites) are observed. These bands disappear at temperatures above 250 °C.

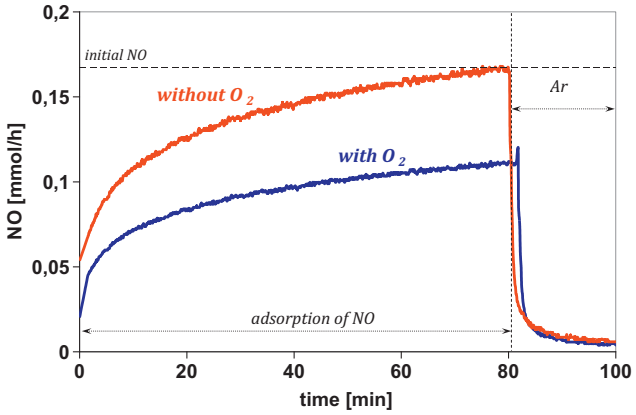

Fig. 5. The adsorption of 250 ppm NO/Ar and 250 ppm NO + 5 vol.% O_2/Ar over $CeZrO_2$.

From this temperature two intensive bands are observed, i.e. a triplet at 1579, 1536 and 1530 cm^{-1} and a band at 1238 cm^{-1}. These bands can be due to formation of mono- and bidentate nitrates. Low intensity bands are observed at 2554, 2231, 1935, 1700, 1032 and 1003 cm^{-1}. According to Davydov [28] the spectral regions for NO adsorption on oxide surfaces are at 1600–1800 cm^{-1} for covalent bonds (M–N=O), 1700–1870 cm^{-1} for coordination bonds (M:NO), 2100–2400 and 1500–1700 cm^{-1} for ionic bonds (M–NO+ and M+NO–) and at 1900–2100 cm^{-1} for ion-coordination bonds. The bands at 1032 and 1003 cm^{-1} can be attributed to $\nu(NO_3^-)$ species [29].

Higher adsorption of NO in the presence of O_2 than in the absence of O_2 can be explained by the formation of different surface species. The adsorption of NO + O_2 on ceria-zirconia yields both the nitrite and nitrate surface species, whereas during adsorption of NO alone, only bridging nitrates are formed. The formation of different surface species can be due to the presence of different oxygen species on ceria-zirconia. The surface peroxide species (O_2^{2-}) are present on ceria-zirconia due to its pretreatment in air at higher temperatures (500 °C). Their presence during NO adsorption leads to formation of bridged bidentate nitrates. The superoxide species (O_2^-) are formed from gaseous oxygen during

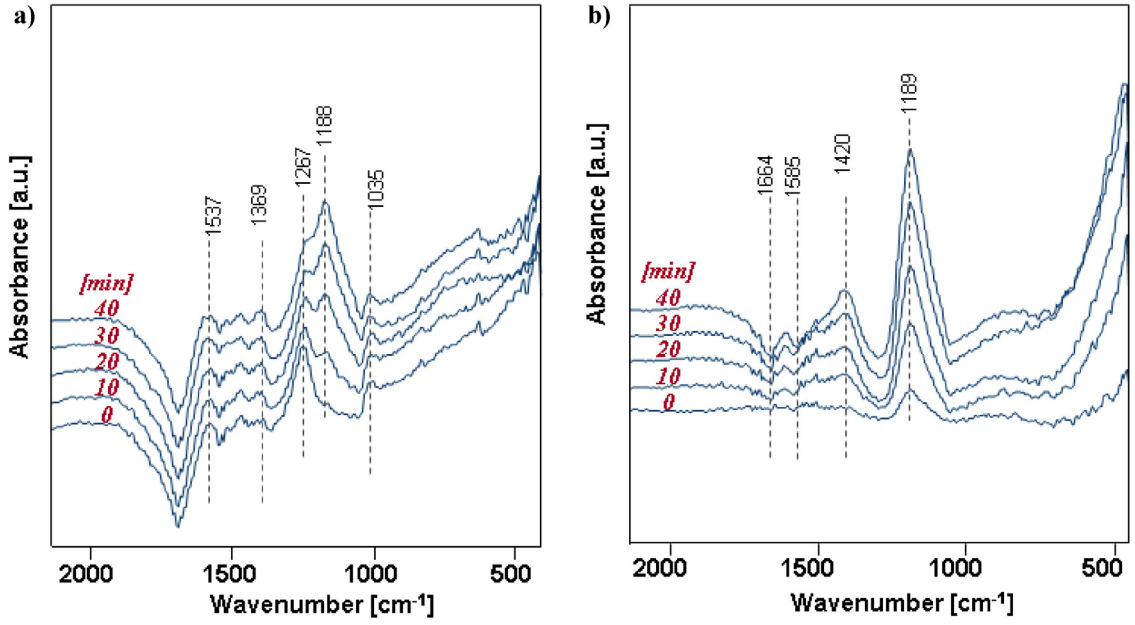

Fig. 6. DRIFTS of CuO/$CeZrO_2$ during the adsorption of (a) 250 ppm NO/Ar and (b) 250 ppm NO + 5 vol.% O_2/Ar.

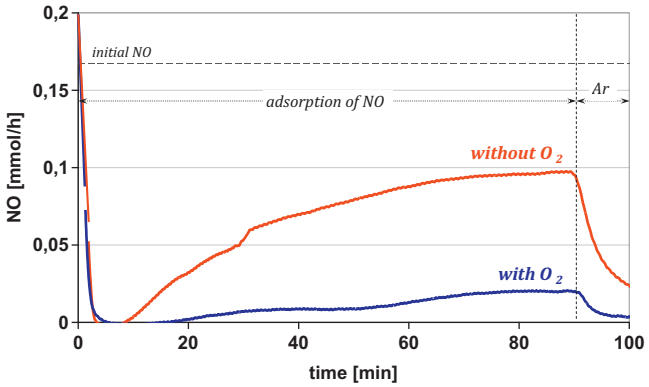

Fig. 7. The adsorption of 250 ppm NO/Ar and 250 ppm NO + 5 vol.% O_2/Ar over $CuO/CeZrO_2$.

$NO + O_2$ adsorption. Superoxide species have high oxidative reactivity at low temperatures, whereas peroxides play a dominant role at higher temperatures [31].

The DRIFT spectra of adsorbed NO-containing species over $CuO/CeZrO_2$ as a function of time of exposure to NO/Ar and $NO + O_2$/Ar at RT are presented in Fig. 6a and b. The DRIFT spectra collected during the adsorption of NO/Ar at RT (Fig. 6a) revealed the presence of three bands, at 1565–1500, 1267 and 1035 cm^{-1}, which according to Davydov [28] correspond to ν_3(N—O) (the two former) and ν_1(N—O) (the latter) stretching modes, respectively. This suggests that NO adsorbs on the catalyst surface to form monodentate nitrato or chelating bidentate nitrato. In this case, NO can adsorb on two CuO sites and be coordinated via N atom. But from the other hand, the bands at 1350–1250 cm^{-1} (ν_s) and 1650–1375 cm^{-1} (ν_{as}) can be also assigned to nitro compounds, in which NO_2^- is coordinated via its N atom. Nitrates are preferentially formed at higher temperatures. Therefore, when the adsorption is carried out at RT, the presence of nitro compounds is more probable. Strong band at 1187 cm^{-1} (ν_{as}(NO)), whose intensity increases in time of NO adsorption, can correspond to the formation of bridging nitro-nitrito (sometimes denoted as chelated nitro species) or monodentate nitrito. However, in the literature this band is usually ascribed to the ν(NO) of nitrites [25,32]. Like in the case of $CeZrO_2$ (Fig. 4) the bands at ca. 1057 and 875 cm^{-1} can be attributed to superoxide (O_2^-) and peroxide species (O_2^{2-}) respectively.

The DRIFT spectra collected during the adsorption of $NO + O_2$/Ar at RT on $CuO/CeZrO_2$ are shown in Fig. 6b. The increase of absorptions at 1420 and 1189 cm^{-1} can be assigned to bridging nitrito (NO_2^-) formed on metal oxide site, adopting the configuration of bridged bidentate ($M_2(O_2)$=N^-) or chelating bidentate ($M(O_2)$=N^-) [20,32–34]. The shoulder at 1550–1500 cm^{-1} may correspond to surface nitrates [35]. The presence of oxygen in the reaction mixture forces specific absorption of NO molecule. Like in the case of $CeZrO_2$ (Fig. 5), the adsorption of NO on $CuO/CeZrO_2$ in the presence of O_2 was higher than when NO was adsorbed alone (Fig. 7). Moreover, the amount of adsorbed NO was higher for $CuO/CeZrO_2$ than for $CeZrO_2$; therefore, the presence of copper enhances NO adsorption.

DRIFT spectra of $CuO/CeZrO_2$ during temperature programmed desorption of pre-adsorbed NO/Ar and $NO + O_2$/Ar are shown in Fig. 8. It is observed in Fig. 8a, that the intensity of the band attributed to the nitrites (at 1184 cm^{-1}) decreases with temperature increase from 50 to 350 °C. The decrease of absorptions at 1227 cm^{-1} (ν_3(N—O)) and 1557 cm^{-1} (ν_1(N—O)), which is observed at 200 and 300 °C, can be ascribed to the loss of bidentate nitrates. A simultaneous increase of absorptions at 1015 cm^{-1} (ν_1(N—O)) and 1450 cm^{-1} can be due to formation of monodentate nitrato (NO_3^-). One can assume that at lower temperatures, the NO, which was adsorbed as a nitrite, desorbs from the catalyst surface. It is observed that from 200 °C the bidentate nitrates disappear, which can be due to their decomposition to monodentate nitrates, because their bands are observed from this temperature. From 350 °C the nitrites are transformed into nitrates.

The DRIFT spectra collected during temperature-programmed desorption of pre-adsorbed $NO + O_2$/Ar are shown in Fig. 8b. It is observed that the most intensive band at 1187 cm^{-1}, which corresponds to nitrito compound (ν_{as}(N—O)), decreases with temperature increase and completely disappears at 400 °C. From 200 °C, the band at 1222 cm^{-1} is observed. This band, combined with weak bands at 1650 cm^{-1} and 1023 cm^{-1} is assigned to monodentate nitrato species (NO_3^-), which are coordinated on metal cation. The increase of absorbance at 1580–1500 cm^{-1} and 1023 cm^{-1} together with band at 1262 cm^{-1}, which shows from 300 °C, corresponds to bidentate nitrato species [20]. Significant desorption of NO_2 from $CuO/CeZrO_2$ surface was observed on the NO-TPD plot from 250 °C (Fig. 3). Thus, it can be concluded that nitrites transform into nitrates with temperature increase. The most stable forms of nitrates are bidentates and their presence on the catalyst surface has been proved by DRIFTS.

Hence, DRIFTS of $CuO/CeZrO_2$ surface during NO-TPD proved that nitrites transform to nitrates when the temperature increases. This observation is in agreement with significant desorption of NO_2 that is observed from 250 °C on NO-TPD profile (Fig. 3). NO_2 is coming from decomposition of surface nitrates. Moreover, DRIFTS has shown that the most stable form of nitrate is bidentate nitrato. Desorption of NO_2 to the gas phase indicates formation of nitrates and is more evident when temperature increases. Nevertheless, due to thermodynamic limitations NO_2 is reduced to NO from 300 °C.

On the basis of DRIFT spectra collected during NO adsorption and NO-TPD, one can assume that oxygen, which is co-adsorbed with NO, plays an important role in formation of surface nitrates. Although bidentate nitrates are preferentially formed on $CuO/CeZrO_2$ in the absence of oxygen at room temperature, they are not created when NO is co-adsorbed with O_2. Therefore, oxygen presence forces the specific form of NO adsorption. As has been mentioned previously, in the presence of O_2, the NO adsorbs via surface superoxides to form nitrites. The nitrates formed in "oxygen-free" conditions probably desorb form catalyst surface as the temperature increases during NO-TPD. Whereas nitrites are transformed into nitrates by the lattice oxygen of ceria-zirconia, but only to some extent. Conversely, nitrites created on the $CuO/CeZrO_2$ surface during adsorption of $NO + O_2$/Ar are easily transformed into nitrates due to a larger amount of oxygen in the ceria-zirconia lattice. Hence, the surface nitrates can be considered as intermediates, which react with hydrocarbon during HC-SCR of NO. Moreover, at low temperatures some part of the nitrites may decompose to NO, whose presence in the gas phase has been observed during the NO-TPD run (Fig. 3d). Desorption of the NO_2, which indicates formation of nitrates, becomes more important when temperature increases. However, above 300 °C NO_2 is reduced to NO due to thermodynamic limitations.

Interaction of toluene with $CuO/CeZrO_2$ and HC-SCR reaction. Fig. 9 shows in situ DRIFTS of $CeZrO_2$ and $CuO/CeZrO_2$ during toluene adsorption and HC-SCR reaction. All experiments were carried out at 250 °C. The experiment carried out in flowing C_7H_8/Ar is in fact a reaction of toluene oxidation due to the high content of oxygen in $CeZrO_2$ and $CuO/CeZrO_2$. Because no bands indicating formation of isocyanates, cyanides, ammonia, amine and ammonium species appeared in the 3800–3100 cm^{-1} and 2300–2100 cm^{-1}, these regions are not shown in Fig. 8a and b. The bands observed in the 3110–2700 cm^{-1} region on both $CeZrO_2$ and $CuO/CeZrO_2$ are assigned to stretching vibrations of the C—H bonds of adsorbed hydrocarbon. Band at 3030 cm^{-1} corresponds to stretching vibrations of C—H of the aromatic ring, whereas stretching vibrations of

the methyl group ν(C—H) are visible in the 3000–2850 cm^{-1} region. Bands of bending C—H in plane occur in 1250–1000 cm^{-1} region but they may overlap with bands assigned to other surface species, formed in reaction of mild oxidation of toluene. The out of plane C—H are not observed in 900–650 cm^{-1} region, hence it is clear that toluene adsorbs on $CeZrO_2$ and $CuO/CeZrO_2$ parallel to the surface. Stretching vibrations of C=O occur at 1600 and 1500 cm^{-1} but in this case they may be overlapped by the absorptions of carbonates (wide, strong band at 1601 cm^{-1}). Moreover, the band at 2740 cm^{-1} that is typical for aldehydes, and the shoulder at 1653 cm^{-1}, which corresponds to C=O stretching vibrations, may be due to formation of benzaldehyde [36]. Toluene can be oxidized to CO_2 and H_2O by the oxygen of ceria-zirconia and CuO. Carbon dioxide can adsorb on the catalyst surface giving carbonates. According to Jacobs [37], bands at 1504, 1360, 1066, 1014 cm^{-1} can be assigned to different types of surface carbonates. The same author ascribes adsorptions

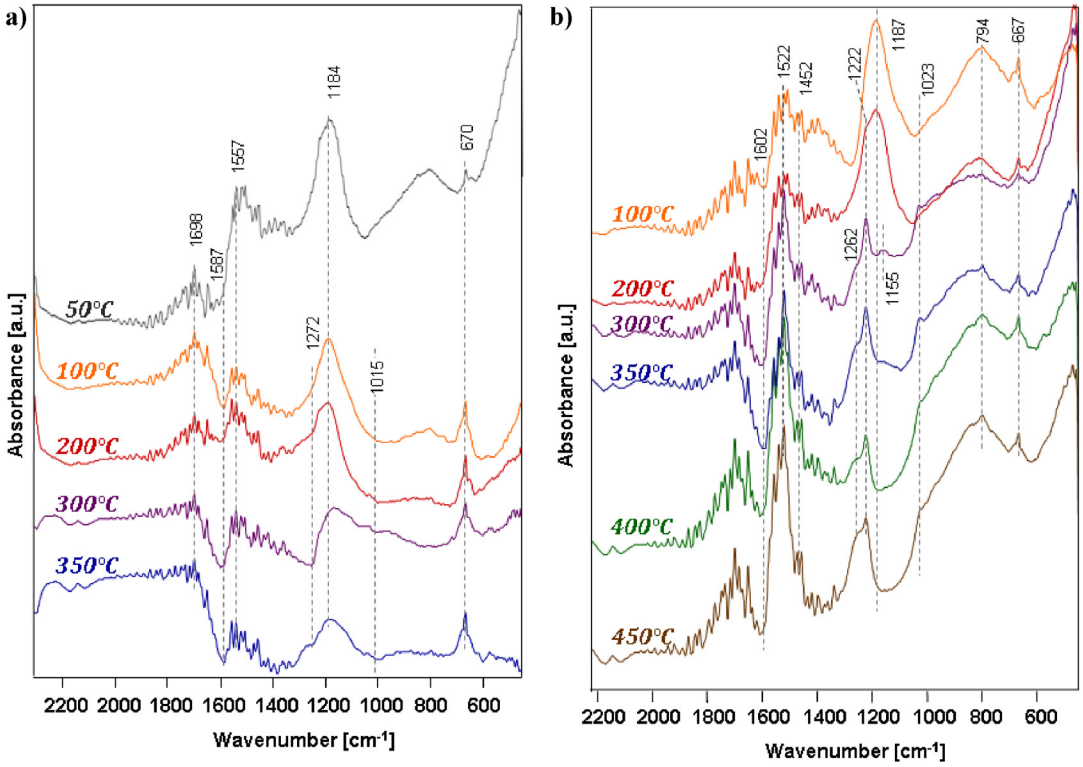

Fig. 8. DRIFTS of $CuO/CeZrO_2$ during temperature programmed desorption of NO in Ar after adsorption of (a) 250 ppm NO/Ar and (b) 250 ppm NO + 5 vol.% O_2/Ar.

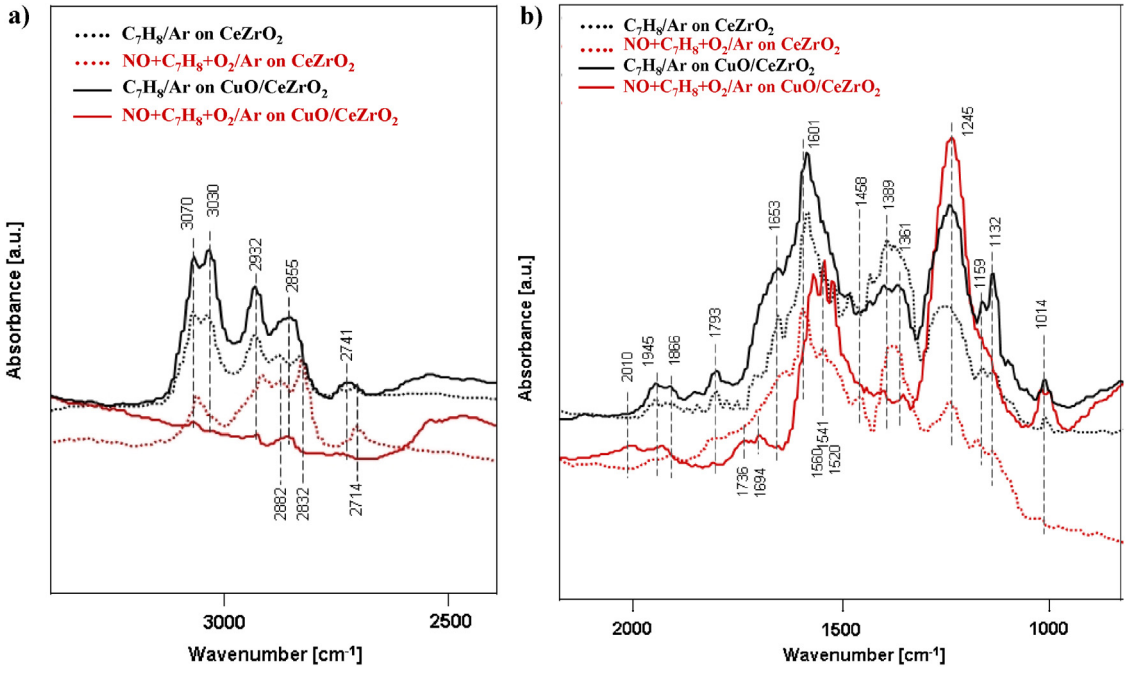

Fig. 9. DRIFTS of $CeZrO_2$ and $CuO/CeZrO_2$ during toluene adsorption (250 ppm C_7H_8/Ar) and HC-SCR reaction (250 ppm NO + 250 ppm C_7H_8 + 5 vol.% O_2/Ar) at 250 °C.

at 2933, 2845, 2723, 1559, 1553, 1542, 1371, 1362 and 1248 cm^{-1} to the surface formates. Arranda et al. [38] assigns bands at 1245 and 1014 cm^{-1} to the surface bidentate carbonates (ν(CO)), while bands at 1450–1350 cm^{-1} to surface bidentate formates (ν(COO)). Carbonates are considered as undesirable surface species during HC-SCR of NO because they may block the active sites of the catalyst. Beside the oxidation to CO_2 and H_2O, toluene can also go through reaction of mild oxidation to oxygenates (alcohols, aldehydes, ketones, carboxylic acids), which may go through the reaction of dimerization. Therefore, bands at 1829 and 1793 cm^{-1} – corresponding to ν(C=O) stretching vibrations, and at 1159–1132 cm^{-1} – assigned to ν(C—O) stretching vibrations, may indicate the formation of anhydrides ($(RCO)_2O$), e.g. phthalic anhydride [39–43]. The oxidation of toluene by the active oxygen of ceria-zirconia or copper oxide can also lead to benzoquinone, whose presence on catalysts surfaces is proven by the occurrence of C=O stretching vibrations at 1653 cm^{-1} [39]. According to Busca [36], toluene is activated on the catalyst surface to benzyl species, which subsequently reacts with the surface of the catalysts giving benzaldehyde, and then is oxidized to carboxylate species (e.g. formates). Reactions of toluene with $CeZrO_2$ and $CuO/CeZrO_2$ proceed similarly. However, the formation of formates is more significant in the case of $CeZrO_2$ and takes place by the cost of carbonates. Inversely, higher formation of carbonates and minor production of formates is observed on $CuO/CeZrO_2$, what is due to the presence of CuO, which is well known for its high activity in oxidation reactions.

DRIFTS of $CeZrO_2$ during HC-SCR reaction carried out at 250 °C show that bands in the 3110–2700 cm^{-1} region, corresponding to the stretching vibration of the C—H bonds of adsorbed toluene are still visible. They decrease significantly during HC-SCR reaction carried out on $CuO/CeZrO_2$, what implies that toluene is consumed in the reaction of NO reduction after the addition of copper to the system. Bands of carbonate species observed in the case of toluene adsorption on $CeZrO_2$ and $CuO/CeZrO_2$ occur at the same wave numbers as bridging nitrates: at 1601 cm^{-1} ($\nu_s(NO_2)$) and 1250 cm^{-1} ($\nu_{as}(NO_2)$). Therefore, IR bands of these species may overlap each other. The band ascribed to surface formates (at 1389 cm^{-1}) is still observed in the case of ceria-zirconia but its intensity significantly decreases when NO reduction assisted by HC is carried out on $CuO/CeZrO_2$. In general, it is observed that formation of surface carbonates and formates on $CuO/CeZrO_2$ is much lower in HC-SCR reaction than during toluene adsorption. Therefore, one can assume that the active sites for NO_x reduction on $CuO/CeZrO_2$ do not suffer inhibition by carboxylate species. The band occurring at 1541 cm^{-1} in the literature is ascribed to RNO_2 [40,42,44], what proves formation nitro organic species according to the assumptions of F2. Bands, which were assigned to oxygenate species during toluene adsorption, e.g. to anhydride (at 1829 and 1793 cm^{-1} and 1159 and 1132 cm^{-1}) decrease in the presence of NO and O_2 as well as the band at 1653 cm^{-1}, corresponding to ν(C=O) of benzoquinone. All bands that prove the occurrence of toluene mild oxidation disappear during reaction of NO_x reduction on $CuO/CeZrO_2$. Hence, it confirms the assumptions of the three-function model of HC-SCR, especially the consumption of oxygenates by NO (F3), which occurs on cationic active sites (Cu^{x+}, Ce^{3+}) (Eq. (6)). In addition, bands observed in 1600–1520 cm^{-1} region are attributed to NO_3^- species and at 1736 and 1694 cm^{-1} can correspond to NO adsorbed on copper cation [29]. Presented DRIFTS of $CeZrO_2$ and $CuO/CeZrO_2$ during HC-SCR reaction carried out at 250 °C revealed that toluene oxidation is more important on copper catalyst. The addition of copper to $CeZrO_2$ shifts the temperature of NO_x reduction into lower values. NO_x reduction assisted by HC can occur on $CeZrO_2$, however copper presence facilitates formation of NO_2, oxygenates and finally N_2. Therefore, copper enhances the efficiency of HC-SCR of NO. However, too high copper loading and formation of big CuO clusters preferentially catalyses the reaction of hydrocarbon total oxidation to CO_2/H_2O, which is competitive reaction to NO_x reduction. It utilizes the reductant, and therefore has negative effect on the efficiency of NO_x reduction.

4. Conclusions

In order to confirm the particular functions in the three-function model of the selective catalytic reduction of NO with the use of toluene, ceria-zirconia supported copper oxide catalyst was tested in four different catalytic runs: NO-TPD, NO_{ox}-TPSR, NO/HC-TPSR and NO/O_2/HC-TPSR. Results of these catalytic runs proved that of all three functions, i.e. F1 – NO oxidation to NO_2, F2 – mild oxidation of toluene to oxygenate (both occurring on CuO and $CeZrO_2$) and F3 – NO reduction to N_2, assisted by total oxidation of oxygenates to CO_2 and H_2O, occurring on Ce^{3+} and copper ions, turn over at the same temperature range. It was determined that the temperature window for SCR of NO with the use of toluene over $CuO/CeZrO_2$ takes place from 215 to 325 °C. The GC analysis revealed formation of N_2 in this temperature range. The selectivity of NO reduction to N_2 was ca. 90%.

DRIFTS revealed that gaseous oxygen enhances adsorption of NO on the surface of ceria-zirconia, which is due to formation of superoxide species (O_2^-). In such a case the NO adsorption yields nitrites and nitrates. The adsorption of NO alone leads to formation of bridging nitrates, due to the presence of surface peroxide species (O_2^{2-}).

The NO adsorbs on $CuO/CeZrO_2$ to form nitrites which are oxidized to nitrates. During HC-SCR reaction, these surface nitrates react with co-adsorbed toluene, giving RNO_2. An unstable nitro organic compound decomposes to NO and oxygenates ($C_xH_yO_z$), which are immediately oxidized to CO_2/H_2O. To achieve high efficiency of studied reaction, oxygenates must react with oxygen left on catalyst surface during NO reduction to N_2. If oxygenates are oxidized by O_2 form the gas phase, the active sites for NO reduction cannot be renovated effectively and the efficiency HC-SCR reaction decreases. DRIFTS of $CeZrO_2$ and $CuO/CeZrO_2$ surfaces in the atmosphere of toluene revealed that this hydrocarbon undergoes mild oxidation to phthalic anhydride and benzoquinone. Presented in this paper DRIFTS confirmed the occurrence of particular functions of SCR of NO with the use of toluene over $CuO/CeZrO_2$.

Acknowledgment

Authors acknowledge the financial support of the International Group of Research (GDRI) “Catalysis for Environment: Depollution, Renewable Energy and Clean Fuels”.

References

[1] H.K. Chagger, J.M. Jones, M. Pourkashanian, A. Williams, A. Owen, G. Fynes, Fuel 78 (1999) 1527–1538.
[2] A. Chmielewski, A. Ostapczuk, J. Licki, K. Kubica, Chemia i Inżynieria Ekologiczna 10 (2003) 1199–1208.
[3] H. Hirano, T. Yamada, K.I. Tanaka, J. Siera, P. Cobden, B.E. Nieuwenhuys, Surface Science 262 (1992) 97–112.
[4] K. Rahkamaa-Tolonen, T. Maunula, M. Lomma, M. Huhtanen, R.L. Keiski, Catalysis Today 100 (2005) 217–222.
[5] V. Parvulescu, P. Granger, B. Delmon, Catalysis Today 46 (1998) 233–316.
[6] F. Garin, Applied Catalysis A 222 (2001) 183–219.
[7] H. Iwakuni, Y. Shinmyou, H. Yano, H. Matsumoto, T. Ishihara, Applied Catalysis B 74 (2007) 299–306.
[8] C. Shi, M. Cheng, Z. Qu, X. Yang, X. Bao, Applied Catalysis B 36 (2002) 173–182.
[9] M. Iwamoto, H. Hamada, Catalysis Today 10 (1991) 57–71.
[10] J.Y. Yan, W.M.H. Sachtler, H.H. Kung, Catalysis Today 33 (1997) 279–290.
[11] M. Iwamoto, H. Yahiro, K. Tanda, N. Mizuno, Y. Mine, S. Kawaga, Journal of Physical Chemistry 95 (1991) 3727–3730.
[12] R. Marques, K. El Kabouss, P. Da Costa, S. Da Costa, F. Delacroix, G. Djega-Mariadassou, Catalysis Today 119 (2007) 166–174.

[13] R. Burch, J.P. Breen, F.C. Meunier, Applied Catalysis B: Environmental 39 (2002) 283–303.
[14] Y. Yeom, M. Li, A. Savara, W. Sachtler, E. Weiz, Catalysis Today 136 (2008) 55–63.
[15] Y.H. Yeom, M. Li, A. Savara, W.M.H. Sachtler, E. Weiz, Journal of Catalysis 238 (2006) 100–110.
[16] F. Meunier, J.R.H. Ross, Applied Catalysis B: Environmental 24 (2000) 23–32.
[17] L.F. Liotta, A. Longo, A. Macaluso, A. Martorana, G. Pantaleo, A.M. Venezia, G. Deganello, Applied Catalysis B: Environmental 48 (2004) 133–149.
[18] G. Centi, P. Fornasiero, M. Graziani, J. Kaspar, F. Vazzana, Topics in Catalysis 16/17 (2001) 173–180.
[19] C. Thomas, O. Gorce, C. Fontaine, J.M. Krafft, F. Villain, G. Djega-Mariadassou, Applied Catalysis B: Environmental 63 (2006) 201–214.
[20] B. Azambre, L. Zenboury, F. Delacroix, J.V. Weber, Catalysis Today 137 (2008) 278–282.
[21] G. Djéga-Mariadassou, Catalysis Today 90 (2004) 27–34.
[22] F. Baudin, P. Da Costa, C. Thomas, S. Calvo, Y. Lendresse, S. Schneider, F. Delacroix, G. Plassat, G. Djega-Mariadassou, Topics in Catalysis 30/31 (2004) 97–101.
[23] G. Djéga-Mariadassou, M. Boudart, Journal of Catalysis 216 (2003) 89–97.
[24] L.F. Liotta, A. Longo, A. Macaluso, A. Martorana, G. Pantaleo, A.M. Venezia, G. Deganello, Applied Catalysis B: Environmental 48 (2004) 133–149.
[25] A. Martinez-Arias, J. Soria, J.C. Conesa, X.L. Seoane, A. Arcoya, R. Cataluna, Journal of the Chemical Society, Faraday Transactions 91 (1995) 1679–1687.
[26] A. Łamacz, A. Krztoń, G. Djéga-Mariadassou, Catalysis Today 176 (2011) 126–130.
[27] W. Zając, Ł. Kurpaska, K. Świerczek, J. Molenda, Ceramic Materials 60 (2008) 234–238.
[28] A. Davydov, Molecular Spectroscopy of Oxide Catalyst Surface: Chapter II: The Nature of Oxide Surface Centers, 2003.
[29] B. Azambre, L. Zenbury, A. Koch, J.V. Weber, Journal of Physical Chemistry C 113 (2009) 13287–13299.
[30] C. Li, K. Domen, K. Maruya, T. Onishi III, Journal of the American Chemical Society (1989) 7683–7687.
[31] Y. Zhao, B.-T. Teng, X.-D. Wen, Y. Zhao, Q. PC, L.-H. Zhao, M.-F. Luo, Journal of Physical Chemistry C 116 (2012) 15986–15991.
[32] K. Hadjiivanov, Catalysis Reviews – Science and Engineering 42 (2000) 71–144.
[33] L. Liu, B. Liu, L. Dong, J. Zhu, H. Wan, K. Sun, B. Zhao, H. Zhu, L. Dong, Y. Chen, Applied Catalysis B: Environmental 90 (2009) 578–586.
[34] M. Kantcheva, E.Z. Ciftlikli, Journal of Physical Chemistry B 106 (2002) 3941–3949.
[35] I. Atribak, B. Azambre, A. Bueno Lopez, A. Garcıa-Garcıa, Applied Catalysis B: Environmental 92 (2009) 126–137.
[36] G. Busca, Catalysis Today 27 (1996) 457–496.
[37] G. Jacobs, R.A. Keogh, B.H. Davis, Journal of Catalysis 245 (2007) 326–337.
[38] A. Aranda, J.M. López, R. Murillo, A.M. Mastral, A. Dejoz, I. Vázquez, B. Solsona, S.H. Taylor, T. García, Journal of Hazardous Materials 171 (2009) 393–399.
[39] D.M. Smith, A.R. Chughtai, Colloids and Surfaces A: Physicochemical and Engineering Aspects 105 (1995) 47–77.
[40] A. Dandekar, R.T.K. Baker, M.A. Vannice, Carbon 36 (1998) 1821–1831.
[41] M.S. Akhter, A.R. Chughtai, D.M. Smith, Journal of Physical Chemistry 88 (1984) 5334–5342.
[42] U. Kirchner, V. Scheer, R. Vogt, Journal of Physical Chemistry A 104 (2000) 8908–8915.
[43] H. Muckenhuber, H. Grothe, Carbon 45 (2007) 321–329.
[44] A. Aissat, S. Siffert, D. Courcot, R. Cousin, A. Aboukaıs, Comptes Rendus de l Academie des Sciences Serie II Fascicule C: Chimie 13 (2010) 515–526.